Paleotsunami deposits along the coast of Egypt correlate with

historical earthquake records of eastern Mediterranean

8
9
10
11

13   Asem Salama, (1, 2, *), Mustapha Meghraoui (1**), Mohamed El Gabry (2, *),

14   Said Maouche (3, *), Hesham Moussa Hussein (2, *), and Ibrahim Korrat (4)

16
17
18   [1.] EOST-IPGS - CNRS - UMR 7516, 5 rue René Descartes, Strasbourg, France
19   [2.] NRIAG, 11421 Helwan, Egypt
20   [3.] CRAAG, Bouzareah, Algeria
21   [4.] Dept. of Seismology, Mansoura University, Mansoura, Egypt

23   * Also at *North Africa Group for Earthquake and Tsunami Studies (NAGET), Ne t40/OEA*
24   *ICTP, Italy*
25
26   **Corresponding author*

38 **Abstract.**

39 We study the sedimentary record of past tsunamis along the coastal area west of Alexandria

40 (NW Egypt) taking into account the occurrence of major historical earthquakes in the eastern

41 Mediterranean. The two selected sites at Kefr Saber (~32-km west of Marsa-Matrouh city)

42 and ~10 km northwest of El Alamein village are coastal lagoons protected by 2 to 20-m-high

43 dunes parallel to the shoreline. Field data were collected by: 1) Coastal geomorphology along

44 estuaries, wedge-protected and dune-protected lagoons, and 2) identification of paleotsunamis

45 deposits and their spatial distribution using five trenches (1.5-m-depth) at Kefr Saber and

46 twelve cores (1 to 2.5-m-depth) at El Alamein. Detailed logging of sedimentary sections were

47 analysed using X rays, grain size and sorting, total organic and inorganic matter, bulk

48 mineralogy, magnetic susceptibility and radiocarbon dating necessary for the identification of

49 past tsunamis records. Generally of low energy, the stratigraphic succession made of marine

50 and alluvial deposits includes intercalated high-energy deposits made of mixed fine and

51 coarse sand with broken shells, interpreted as catastrophic layers correlated with tsunami

52 deposits. Although the radiocarbon dating of 46 samples consist in mixed old (> 13000 year

53 BP) and young (< 5500 year BP), dated charcoal and shell in sedimentary units allow the

54 correlation with the 24 June 1870 (Mw 7.5), 8 August 1303 (Mw ~8) and 21 July 365 (Mw 8

55 – 8.5) large tsunamigenic earthquakes that caused inundations in Alexandria and northern

56 Egyptian shoreline. Our results point out the size and recurrence of past tsunamis and the

57 potential for tsunami hazard over the Egyptian coastline and the eastern Mediterranean

58 regions.

59

60

61

1. Introduction:

62

63 Egypt has a well-documented historical catalogue of earthquakes and tsunamis

64 recorded in ancient texts and manuscripts. Original documents and archives from past

65 civilizations are considered as the principal sources of macroseismic data for major historical

66 earthquakes and tsunamis (Poirier and Taher, 1980; Maamoun et al., 1984; Ambraseys et al.,

67 1994, 2009; Guidoboni et al., 1994, 2005; Soloviev et al. 2000, Tinti et al., 2001). The

68 catalogue of Ambraseys et al., 2009 reports that coastal cities of northern Egypt have

69 experienced repeated tsunamis inundations with severe damage in the past. While historical

70 earthquakes and tsunamis are well documented, it appears that there is a lack of holistic

71 investigations for tsunami deposits along the Mediterranean coastlines. The geomorphology

72 along the Mediterranean coastline of northern Egypt with low-level topography (Hassouba,

73 1995), dunes and lagoons constitutes an ideal natural environment for the geological record of

74 past tsunamis.

75 The Eastern Mediterranean region experienced major earthquakes (with Mw > 7.5)

76 mainly along the Hellenic subduction zone due to the convergence between the Eurasian and

77 African plates (Fig. 1; Ambraseys et al., 1994, Taymaz et al., 2004). Major historical tsunamis

78 in the eastern Mediterranean region that affected northern Egypt are triggered by large

79 earthquakes (Papadopoulos et al., 2014) but the possibility of landslide tsunami associated

80 with local earthquakes (El-Sayed et al., 2004) may also exist. Yalciner et al. (2014) estimated

81 that up to 500 km^3 landslide volume, with wave height ranging from 0.4 to 4 m, might have

82 taken place offshore the Nile Delta. However, the effects of landslide tsunami are limited to

83 the nearby coastline as shown by the recent examples of landslide tsunamis in the

84 Mediterranean (Tinti et al., 2005).

85 Tsunami research of the past 20 years has led to the discovery of coastal tsunami

86 sedimentary records dating back to thousands of years. Among the early studies, the evidence

87 of more than 6 soil levels buried below tsunami deposits in the past 7000 years were found at

88 Puget Sound coastline of Washington state (Atwater, 1987). Nanayama et al. (2003)

89 recognized major tsunamis due to extensive coastal inundation along the eastern coast of

90 Hokkaido (northern Japan); the repeated sand sheet layers several kilometres inland evidenced

91 a 500-year tsunami cycle in the period between 2000 and 7000 years BP. Following the 2004

92 Sumatra earthquake (Mw 9.1) and tsunami, Malik et al. (2015) identified in trenches three

93 historical tsunamis during the past 1000 years along the coast of South Andaman Island

94 (India). In the Mediterranean, De Martini et al. (2012) identified two tsunamis deposits

95 during the first millennium BC and another one in 650-770 AD and estimated 385 year

96 average recurrence interval for strong tsunamis along the eastern coast of Sicily (Italy).

97   In this paper, we investigate the paleotsunami deposits in the northern coast of Egypt

98 and their correlation with the historical tsunami catalogue of the Eastern Mediterranean.

99 Using coastal geomorphology with trenching and coring, we examine the geological evidence

100 of tsunami deposits using geochemical analysis, magnetic susceptibility and radiocarbon

101 dating to identify the tsunamis records. The Bayesian simulation (Oxcal 4.2; Bronk-Ramsey,

102 2013) is applied to the radiocarbon results and stratigraphic succession of coastal deposits in

103 order to generate a precise paleochronology of tsunami events. Finally, we discuss the

104 evidence of paleotsunamis and their dating in comparison with the major historical

105 tsunamigenic earthquakes of the Hellenic and Cyprus subduction zones.

106

107 **2. Major historical tsunamis of the Mediterranean coast of Egypt**

108   The tsunami catalogue of Egypt cites the work of Guidoboni et al. (1994, 2005) and

109 Ambraseys (2009) that report several large historical tsunamigenic earthquakes with severe

110 damage in the eastern Mediterranean regions (Table 1). Among these events, the tsunamis of

111 21 July 365, 8 August 1303 and 24 June 1870 inundated the harbour of Alexandria city as

112 well as the Mediterranean coast of Egypt.

113   Early in the morning of 21 July 365, an earthquake with estimated magnitude ~Mw 8-

114 8.5 located offshore West of Crete generated a major tsunami that affected the eastern

115 Mediterranean coastal regions (Ambraseys et al., 1994). A contemporaneous account from the

116 Roman historian Ammianus Marcellinus (born 325 – 330, died c. 391 – 400; Guidoboni et al.,

117 1994) reported the sudden retreat of the sea and the occurrence of a "gigantic" wave inland

118 with inundation and damage to the Alexandria harbour and city where ships were lifted inland

119 on house roofs; the estimated wave height of this tsunami was calculated by Hamouda (2009)

120 to be larger than 8 m in Alexandria. The seismic source of this earthquake is located in west

121 Crete, according to archeological and historical damage distribution, combined with coastal

122 uplift measurements and modelling (Fig. 1; Guidoboni et al., 1994; Stiros, 2001; Shaw et al.,

123 2008 and Ambraseys, 2009).

124   On 8 August 1303 a major earthquake with magnitude ~Mw 8 located in between

125 Crete and Rhodos islands generated a tsunami that greatly damaged the coastal cities of the

126 eastern Mediterranean (Guidoboni and Comastri, 2005; Ambraseys, 2009). Abu-El Fida

127 (1907) reported in 1329 that the Alexandria city and Nile delta were flooded and many houses

128 were damaged in Cairo and northern Egypt. In Alexandria, part of the city walls collapsed, the

129 famous lighthouse was destroyed and some ships were torn apart carried up inland due to the

130 tsunami waves (Abu-El Fida, 1907). In a recent synthesis of major seismic sources,

131 Papadopoulos et al. (2014) locate the 1303 earthquake in between Crete and Rhodos Islands

132 of the Hellenic subduction zone (Fig. 1).

133   On 24 June 1870, a large earthquake affected many places of the eastern

134 Mediterranean region and was felt in Alexandria at around 18 h with no damage in the city

135 but with slight damage in Cairo (Ambraseys, 2009). In Alexandria coastline and Nile Delta,

136 the sea wave flooded the quays of ports and inland fields (Coumbary, 1870). The seismic

137 source location of this earthquake at the eastern edge of Crete is inferred from the damage in

138 Heraklion and felt shaking around the east Mediterranean (Fig. 1; Schmidt, J.F., 1879;

139 Jusseret and Sintubin, 2017).

140   Among these three reported earthquakes, it appears that the AD 365 and AD 1303 that

141 can be classified as very large earthquakes (with Mw ≥ 8; Stiros, 2001; Shaw et al., 2008;

142 Hamouda, 2006, 2009) generated major tsunamis with basin-wide impacts, while the 1870

143 earthquake may be of a lower magnitude (Mw ~7 – 7.5; Ben Menahem et al., 1991; Soloviev,

144 2000). Several studies of the 21 July 365 and 8 August 1303 historical earthquakes refer to

145 tsunami waves with inundation in Alexandria and coastlines of northern Egypt, and therefore

146 with the potential of tsunami records in the sedimentary deposits. However, there have been

147 some debates on the 1870 event concerning its location, size and the possibility of tsunami

148 waves, but several authors (Soloviev et al., 2000; Ben Menahem et al., 1979; Salamon et al.,

149 2007; Papadopoulos et al., 2010; and Maramai et al., 2014) support the tsunami generation by

150 1870 earthquake.

151

152 **3. Coastal geomorphology and site selection of paleotsunami records**

153   The northwest Mediterranean coast of Egypt forms the northern extremity of the

154 Marmarica plateau which is a Miocene homoclinal limestone that extends west of Alexandria

155 for about 500 km, acting as a major catchment area feeding the drainage system (Fig. 1). The

156 plateau runs from the Qattara Depression southward to the piedmont plain northward with

157 various elevations reaching ~100 m at Marsa Matrouh escarpment. The geomorphological

158 landform of the study area is characterized by a 60-m-high northern plateau that includes

159 ridges, sand dunes, lagoons, and rocky plains within a 20-km-wide strip along the coastline

160   (Fig. 1). The rocky Pleistocene limestone ridges include a veneer of carbonate sand that are

161   mostly composed of oolitic grains (Frihy et al., 2010).

162   Coastal dune-ridges protect inner lagoons from the sea and constitute outstanding

163   landform features at several locations parallel to the shoreline (Figs 2 and 3). These dunes are

164   weathered where the rocky headlands outcrop (Abbas et al., 2008). The 2 to 20-m-high

165   coastal beach-dune ridge mainly composed of oolitic and biogenic calcareous sand separates

166   coastal lagoons and *sabkhas* (salt lake) from the sea. The beach-dune ridge is developed along

167   the receding Quaternary shorelines and embayment of the Mediterranean Sea (Hassouba,

168   1995). The lagoons with flat depressions separated from the sea by the coastal dunes (with

169   different heights and sometimes with seawater outlets) are designated sites for the record of

170   past tsunami deposits.

171   The accumulation of large boulders (Shah-Hosseini et al., 2016) near the selected sites

172   is considered as a possible witness of past tsunami events. However, the boulders along the

173   coastlines may either results from storms (Hall et al. 2006; Spiske et al. 2008) or tsunami

174   waves (Goff et al. 2006; 2009; Morhange et al. 2006). The majority of boulders observed near

175   our investigated sites shows imbricated positions of large blocks directed toward south, a

176   situation comparable to the tsunamigenic boulders studied along the Algerian coastline

177   (Maouche et al. 2009).

178   The discrimination between storm and tsunami deposits is a challenge in the

179   Mediterranean regions (Maouche et al., 2009; Marriner et al., 2017). However, the tsunami

180   stratigraphic record is less frequent (according to Tinti et al., 2001) and often presents a

181   specific sedimentary signature with mixed deposits that include: 1) The basal contact of

182   tsunami layer is extremely sharp with loading structures where layers contain organic rich

183   mud and vegetation (Matsumoto et al., 2008; Switzer and Jones 2008); 2) the presence of rip

184   up clasts that also suggest considerable erosion of lagoon deposits usually associated with

185   tsunami deposits (Szezucinski et al 2006); 3) The tsunami deposits tend to be much more

186   poorly sorted than storm deposits (Paris et al., 2007); 4) the large number of mixed and often

187   broken bivalve and shells that occupy large vertical and lateral stratigraphic positions (Donato

188   et al., 2008); 5) the tsunami deposits tend to have laminations and or cross bedding due to

189   landward or seaward current (Tuttle et al., 2004); 6) the particle sizes of tsunami sediments

190   fine landward from the shores (Srinivasalu et al., 2009); 7) the grain size are often bimodal

191   particles size than the storm which tend to have unimodal particle size (Paris et al., 2007); 8)

192   The increase of concentrations of Na, S, Cl, Mg with the presence of heavy minerals in

193   tsunami deposits (Szczucinski et al., 2006; Babu et al., 2007); and 9) The low peak value of

194   magnetic susceptibility linked to the amount of sand originated from the littoral dunes and

195   reworked mixed sediments from tsunami waves (Font et al., 2010).

196   The local geomorphological and topographic settings contribute to the site selection

197   for paleotsunami investigations. Our site selection for trenching and coring took into account

198   the accessibility to dry lagoons (during summer season) in areas with no urbanization or

199   artificially reworked soil. Suitable sites for trenching and coring are located in areas protected

200   from the sea by the rather low (~2-m-high) sand dune topography that allows tsunami waves

201   and related material to deposit into the lagoon. Two ~200 km apart sites of seasonal dry

202   lagoons have met the selection criteria for paleotsunami investigation (Figs. 1 and 2): 1) Kefr

203   Saber located at ~32-km west of Marsa-Matrouh city, and 2) El Alamein site at ~10 km

204   northwest of El Alamein city and ~150 km west of Alexandria. Five trenches were dug at

205   Kefr Saber (Fig 2a), and 12 cores were performed at the El Alamein site (Fig 2b).

206

207   4. Used methods for paleotsunami investigations

208   The trench size is ~2 x 1 meter with ~1.5-m-depth depending on the water table reach;

209   all trench walls exposed fine-grained sedimentary layers and were logged in details. The

210   maximum core depth is ~2.6 m and their distribution in the lagoons was planned to occupy an

211   area from the depression (depo-centre) to the edge close to the outlet of seawater in order to

212   observe any thickness variation of tsunami layers.

213   The core tubes were split in half lengthwise, photographed using both normal and

214   ultra-violet lightning accompanied by detail description of textures and sedimentary

215   structures. An X-ray scanning was performed immediately after core opening and all cores

216   were sent to the laboratory of the National Institute of Geophysics and Astronomy (NRIAG,

217   Cairo) for sampling and further analysis. The magnetic susceptibility measurements were

218   operated along cores and samples were collected for radiocarbon dating, physical, chemical

219   and organic matter analyses.

220   The magnetic susceptibility was measured for cores at the NRIAG Rock Magnetism

221   laboratory then corrected against air by using Bartington compatible software. 120 samples

222   were collected from cores then analysed for grain size analysis; X-ray diffraction using

223   Philips PW 1730. The total organic and inorganic measurements were carried out at the

224   laboratory of Central Metallurgical Research & Development Institute (CMRDI at Eltebbin,

225   Egypt). Statistics of the grain-size distribution were calculated using Folk equations (1968) to

226   obtain mean size and sorting of the sediments along the cores.

227   The Radiocarbon dating of samples are carried out in three laboratories (Poznan

228   laboratory - Poland, CIRAM in Bordeaux, France and Beta Analytical laboratory, USA) to

229   ensure coherency and quality of results (see Tables 2 a and b). The collected samples are

230   made of charcoal, bones, gastropods, shells and organic matter. The radiocarbon dating results

231   of samples are subsequently corrected using a recent calibration curve (Reimer et al., 2013)

232   and the Oxcal software (Bronk-Ramsay, 2009) for the probability density function with 2σ

233   uncertainty for each dated sample. In addition, from a succession of calibrated dates, a

234   Bayesian analysis provides the simulated age in probability density function of a catastrophic

235 event. The simulated age allows the correlation between the tsunami layer deposits, the

236 related isotopic chronology and the historical tsunami events in catalogues.

237

238 **5. Description of trenches and cores sedimentary layers**

239 The selected sites revealed a succession of sedimentary units typical of lagoon

240 deposits with fine strata made of a mix of fine gravel, sand, silt and clay (Salama, 2017). At

241 both Kefr Saber and El Alamein sites, trenches and cores present comparable soft sediment

242 content and stratigraphy. The variation of sediments content in the different cores is due to the

243 distance from the shore and to the core location in the lagoons with regard to dunes heights. A

244 detailed description of the trenches and cores at both Kefr Saber and El Alamein sites is

245 presented here below:

246 **5. 1. Kefr Saber site:** Trenches P1, P2, P3 and P4 are 20 to 40 m distance, have quite

247 similar sedimentary succession with fine-grained mostly alluvial deposits made of sandy-silty

248 layers with mixed coarse and white fine sand that contains broken shells of marine origin

249 (Fig. 3 and trench logs in supplemental material S1). A conspicuous layer of white mixed

250 sand, gravel and broken shells with variable 2 to 15 cm thicknesses is found at 30 – 50 cm

251 depth in P1, P2, P3; its thickness decreases landward to 1 cm in P4 (see supplemental material

252 S1 a, b, c, d, e). Trench P5 which is close to the dunes and shoreline shows a succession of

253 coarse and fine sand, and 30 to 40 cm thick mixed with pebbles which, as observed in other

254 trenches, are fining inland. According to Goff et al., 2006, the high energy fining inland

255 sedimentary sequence is related to tsunami deposits rather than storm deposits. The white

256 mixed sand with broke shells characterized by high-energy sedimentary deposits is interpreted

257 as of tsunami origin.

258 The mixed radiocarbon dating of samples in trenches is an issue at Kefr Saber. Two

259 charcoal samples collected in Trench P1 at 35 cm and 53 cm depth display modern age

260   (younger than 1650 AD) and 39000-38250 BC, respectively. In Trench P2, two other charcoal

261   samples collected at 73 cm and 100 cm depth and both below the tsunami layer labelled 1

262   (Fig. S1-b) indicate 50 - 70 AD and 5300-5070 BC, respectively (see also Table 2a). In

263   Trench P4, four collected charcoal samples at 15 cm, 25 cm, 40 cm and 61 cm depth reveal

264   modern ages (younger than 1650 AD). A fifth charcoal sample located at 60 cm depth

265   provides 17200- 15900 BC. In Trench P5, four charcoal samples are collected with the

266   uppermost sample located at 12 cm depth is dated at 360-50 BC, the second sample at 17 cm

267   depth show 30- 180 AD, the third, and fourth charcoal samples found at 33 cm and 37 cm

268   depth are dated at 350 - 1050 BC and 2400-4000BC, respectively. The mixing between old

269   (older than 7000 years BP) and relatively young ages (younger than 2000 years BP) denotes

270   of the deposit of reworked layers within an environment of young sedimentation in lagoon.

271   *Results:* Although the sedimentary deposits in trenches at Kefr Saber indicate mixed

272   and reworked sedimentation, the well identified coarse and fine white sand layer with broken

273   shells of marine origin located ~ 30 - 73 cm depth in all trenches P1 to P4 suggests a single

274   homogeneous sedimentary unit of relatively young age deposited in the lagoon. Considering

275   that the stratigraphic succession and related chronology are comparable in all trenches dug in

276   the same lagoon, we selected the radiocarbon dates younger than 2000 year BP that bracket

277   the white sandy layer unit (i.e., samples TSU P5 S4 and S5, TSU P3 S1 and S3 that predate

278   the unit, and sample TSU P3 S2 that postdates the unit). The Oxcal dating simulation provides

279   the 137 – 422 AD bracket of the white sandy layer unit that may be correlated with the

280   tsunami deposits of the 21 July 365 earthquake (Fig. 4).

281   North of the trench sites at Kefr Saber, the dating of shells (Dendropoma) of a sample

282   collected in a large boulder provide a radiocarbon calibrated date of 940-1446 AD. The dating

283   of Dendropoma collected in a boulder often marks the catastrophic coastal environmental

284   change with displaced large boulders from an intertidal to shoreline position due to a tsunami

285   event (Goff et al., 2012). The Dendropoma sample age at Kefr Saber may correlate with the 8

286   August 1303 earthquake and tsunami event that dragged large boulders on the shoreline in

287   agreement with the results of Shah-Hosseini et al. (2016). However, we could not identify the

288   1303 event in the trenches dug in the nearby lagoon at Kefr Saber.

289   **5. 2. El Alamein site***: The 12 cores extend between 1 m and 2.6 m depth and except

290   for cores 1 and 9 which are shown in Figures 5 a and b, the detailed stratigraphic logs and

291   related measurements are presented in the supplemental material S2. In a previous

292   reconnaissance field investigation, a coarse and fine white sand layer was identified ~ 30 cm

293   depth in a test pit. Two charcoal samples El Al sa1 and El Al sa2 collected at 25 cm and 56

294   cm depth give 1680-1908 AD and 1661-1931 AD ages, respectively. The description of cores

295   is as following:

296   **Core 1:** This core is located at ~166 m from the shoreline (Fig. 2 b), east of the study area

297   behind the sand dunes and near the outlet of the seawater. The core depth reached ~2.14 m

298   and the stratigraphic section includes 3 tsunami layers recognized as following (Fig. 5 a

299   section 1 and its continuation at depth in Fig. S2-1):

300   The first layer is at ~12.5 cm depth with ~34.5 thick, brown clay sediments with poor sorting,

301   fine grain sediments, with high peak in magnetic susceptibility, rich in organic matter, and X-

302   ray image reflects clear lamination. The second layer which is located at ~70 cm depth has ~5

303   cm thickness, characterized by highly broken shells fragments with the extremely bad sorting

304   of sediments granulometry. The third layer at ~75 m depth is ~22 cm thick, made of pale

305   yellow sand with bad sorting of sediments size, and a peak in magnetic susceptibility. The

306   chemical analysis shows the presence of gypsum and minor goethite, and X-ray scanning

307   shows some turbiditic structures. A fourth tsunami layer is identified at 158 cm (see Fig. S2-1;

308   section 2). It is characterized by pale brown silty clay, with broken shells fragments and

309   extremely poor sorting, and with a high peak of magnetic susceptibility.

Two samples were collected for radiocarbon dating from core 1. The first and uppermost sample is a charcoal fragment at 40 cm depth located within a layer of catastrophic mixed sedimentary unit characterized by bad sorting, highly broken shells fragments and the peak of magnetic susceptibility. We interpret this layer as of tsunami origin and although its stratigraphy is located close to the surface, the mixed and reworked sedimentation explains the obtained old age 13985- 14415 BC (Table 2b). The second sample is a rodent bone at 50 cm depth and provides 403-603 AD calibrated age that postdate a catastrophic layer made of white sandy layer with broken shells. This catastrophic layer may correlate well with the 365 AD major earthquake of the eastern Mediterranean.

Core 2: As shown in core 2 is ~90 cm deep located south of core 1 at ~264 m from the shoreline (Fig. 2 b, Fig. S2 – 2). Two tsunami layers are identified. The first tsunami layer is ~12 cm thick brown clay sediments at ~13 cm depth, mixed with gravel and sand. The layer is rich in organic matter (> 1), with a small peak of magnetic susceptibility and where the geochemical analysis shows a minor component of goethite. The second layer at ~50 cm depth is ~15 cm thick, made of mixed yellow sand with silty-clay pockets, broken shells fragments, poor sorting and with peak magnetic susceptibility. It is rich in organic matter comparing to the other layer, and the geochemical analysis shows minor component of halite.

Several samples were collected below and above the tsunami layers but, unfortunately, their content did not deliver enough carbon for dating. The two shells (gastropod) samples collected at 75 cm and 77 cm depth (well below the lowermost tsunami layer, Fig.S2-2) have calibrated dates 32971-34681 and 34362-36931 BC, respectively (Table 2b). These obtained ages may well be due to a mixed and/or reworked sedimentation.

Core 3: This core is located at 270 m from the shoreline and the outlet of sea water has revealed three tsunami layers (Fig. 2b and Fig. S2 – 3). The first tsunami layer is at ~25 cm depth and corresponds to 26 cm thick pale brown clay characterized by broken shells

335 fragments and sediments rich in organic matter. The second layer at ~70 cm depth is 17.5 cm

336 thick characterized by white sand laminated at the top with a peak of magnetic susceptibility

337 near zero value, and with high organic matter > 2. The third tsunami layer at 106 cm depth is

338 32 cm thick, characterized by yellow sand with minor illite and broken shells fragments.

339   Two shell samples were collected for dating at 37 cm and 45 cm depth and show

340 calibrated dates 43618 BC and 34218-37224 BC respectively (Fig.S2-3 and Table 2b). These

341 two samples are located within the stratigraphic tsunami layer 2 and may correspond to

342 reworked sediments due to the high energy sedimentation during the catastrophic event.

343 **Core 4:** The core is located at 435 m from the shoreline and shows sedimentary units where

344 we identify two tsunami layers with high magnetic susceptibility (Fig. S2 - 4). The first

345 tsunami layer is the white sand at ~12.5 cm depth 7 cm thick with poorly sorted sediments,

346 broken shells fragments with organic matter > 2. The second tsunami layer is a pale yellow

347 sand at ~102 to 130 cm depth, characterized by broken shell fragments in a yellow sand with

348 a minor amount of illite and gypsum.

349   One shell sample collected for dating at 37 cm depth provides a calibrated date 32887-

350 34447 BC respectively (Table 2b). This sample located in the stratigraphic tsunami layer 1

351 apparently results from high energy reworked sedimentation during the catastrophic event

352 (Fig. S2-4).

353 **Core 5:** This is the southernmost core in the El Alamein site, located at 490 m distance from

354 the shoreline (Fig. 2 b; Fig. S2 - 5). The core reaches 73 cm depth and the sedimentary

355 succession does not show any possible catastrophic sedimentary layer of tsunami origin.

356 According to its content, core 5 may show the limit of inundation area with respect to at least

357 the first and second tsunami layers.

358 **Core 6:** This core is located south of the sand dunes at 320 m from the shoreline (Fig. 2 b). It

359 is characterized by three tsunami layers (Fig. S2 - 6). The first tsunami layer is a ~24 cm thick

pale yellow sand with broken shells fragments (between 5 and 26 cm depth) and poorly sorted sediments rich in organic matter (larger than 2.5). The second tsunami layer is ~18.5 cm thick at 50 - 75 cm depth characterized by yellow sand with mixed gastropods and bivalves, and a high value of magnetic susceptibility. The third tsunami layer at 130 cm depth is ~20 cm thick, rich in organic matter, characterized by white sand mixed with gravel and pebble and broken shells fragments.

Three samples were collected for dating in core 6. The first sample is a gastropod at ~45 cm depth and shows 35002-37441 BC calibrated date. The second and third samples are coral fragments at ~60 cm and ~80 cm depth that gave 42776-69225 BC and modern (younger than 1650AD) calibrated ages. The first sample is above the tsunami layer 2 while the second sample was within the stratigraphic tsunami layer 2 (Fig S2-7). These samples may result from mixed sedimentation and reworking due to high current waves transport of tsunamis.

Core 7: This core was located at 273 m from the shoreline (Fig. 2 b). It is characterized by sedimentary units that may include three tsunami layers within 120 cm core depth (Fig. S2 - 7). The first tsunami layer is a 6 cm thick brown sand with broken shell fragments at ~14 cm depth and a considerable amount of gypsum with a minor amount of Illite and goethite. It is rich with organic matter (> 2) of a swampy environment and the noticeable peak of magnetic susceptibility. The second tsunami layer at 50 cm depth is 20 cm thick, characterized by laminated pale brown clay mixed with gravel and pebbles at the bottom. The third tsunami layer is 15 cm thick at 115 cm depth characterized by white sand, bad sorting sediments with aminor amount of pyrite.

A single sample of shell fragment collected at 17 cm depth for radiocarbon dating within tsunami layer 1 provides 293-1113 BC.

Core 8: This core is located at 214 m from the shoreline (Fig. 2 b). Three tsunami layers are recognized (Fig. S2 - 8). The first tsunami layer is 16 cm thick pale silty clay at ~14 cm depth, rich in organic matter, with minor amount of goethite, characterized by highly broken shell fragments. The second layer is a 22 cm thick at ~52 cm depth, of pale yellow silty-clay with broken shells, characterized by a high peak of magnetic susceptibility and rich inorganic matter (>2.5). The third tsunami layer is 9 cm thick at ~128 cm depth, characterized by pale yellow sand with broken shells fragments and badly sorted angular gravel sediments. No samples were suitable for dating in this core.

Core 9: The core is located at 130 m from the shoreline. Three tsunami layers are recognized (Fig. 5 b; Fig. S2 - 9). The first tsunami layer is white sand at ~16 cm depth and 13 cm thick with ahigh content of organic matter and rips up clasts that appear in X-ray scanning characterized by highly broken shells fragments and rich in organic matter. The second layer at 67 cm depth is 22 cm thick characterized by white sand, with a peak of magnetic susceptibility, high content of organic matter larger than 5. The third tsunami layer at 139 cm depth is 14 cm thick characterized by broken shells fragments and white sand with highly angular sediments that reflect the bad granulometric sorting.

Two samples were collected for dating in core 9. The first sample is a gastropod shell located at 24 cm depth within the tsunami layer 1 that gives 1052-1888 BC calibrated age. The second sample at 55 cm depth is a bivalve (lamellibranch) located above the tsunami layer 2 dated at 40521-43169 BC calibrated age. These samples may have been transported and re-deposited due to high current waves of the tsunami events.

Core 10: The core is located at 245 m from the shoreline (Fig. 2 b). Three tsunami layers are recognized (Fig. S2 - 10). The first tsunami layer is 9 cm thick brown silty clay, at ~19 cm depth with broken shells fragments, rich in organic matter (> 4) and high peak of magnetic susceptibility; rip up clasts and laminations appear in X-ray scanning. The second layer 38 cm

409   thick brown sand at 48 cm depth with broken fragments of shells, peak of magnetic

410   susceptibility and high organic matter (> 1.5) at the bottom of the layer. The third tsunami

411   layer is 28 cm thick pale yellow sand at 101 cm depth characterized by rich organic matter

412   and sediments that reflect the bad sorting.

413   Two samples were collected for dating in core 10. The first sample located in the

414   tsunami layer 1 is a shell fragment at 24 cm depth that gives 2623-3521 BC calibrated age.

415   The second sample located in the tsunami layer 2 is a rodent bone at 70 cm depthshowing

416   41256-46581 BC calibrated age (see also Table 2b). Both samples may result from reworked

417   sedimentary units due to high current waves of tsunami events.

418   **Core 11:** The core is located at 151 m from the shoreline (Fig. 2 b). Three tsunami layers are

419   recognized (Fig.S2 - 11). The first tsunami layer is 10 cm thick white sand with broken shell

420   fragments at ~19 cm depth; the layer also shows high magnetic susceptibility, rich organic

421   matter (> 4) with a high percent of gypsum (>50%). The second layer is 9 cm thick white

422   sand at 76 cm depth, with broken shell fragments, a high peak of magnetic susceptibility and

423   organic matter larger than 1.5. The third tsunami layer is 21 cm thick grey silty sand, with

424   broken shell fragments at 107 cm depth; bad sorting, high organic rich matter and a minor

425   amount of Illite and gypsum.

426   Eight samples were collected for dating in core 11. The sedimentary units at 112 - 175

427   cm depth (core bottom) and related succession of ages between 3943 BC and 2475 BC (from

428   shell gastropods and a charcoal fragment; see Table 2 b), may indicate a consistent dating of

429   the tsunami layer 3. However, the first sample (gastropod shell) at ~20 cm depth that gives

430   3638-4328 BC, the second sample (broken shell) at 62 cm depth with an age at 17869 - 18741

431   BC, and the 33294 – 36120 BC and 2619 – 3386 BC out of sequence dating (Table 2 b)

432   indicate samples of transported and reworked shells and sediments probably due to high

433   energy tsunami deposits.

434 **Core 12:** The core is located at 127 m from the shoreline (Fig 2 b). Three tsunami layers are

435 recognized in section 1 and one tsunami layer in section 2 (Fig. S2 – 12 a, b). The first layer is

436 ~7.5-cm-thick at ~19-cm-depth and is made of poorly sorted white sandy deposits, and highly

437 broken gastropods and lamellibranch fossils. The layer is characterized by high values of

438 organic matter and magnetic susceptibility. The second layer is ~13-cm-thick white sandy

439 deposits intercalated with coarse brown sand at ~32.5-cm-depth, characterized by horizontal

440 lamination, poor sorting sediments, rich in organic matter and high peak of magnetic

441 susceptibility. The third layer is ~25-cm-thick grey sandy clay at 89-cm-depth, with

442 laminations at the bottom of deposits, vertically aligned gastropods, broken shells fragments,

443 rich in total organic matter and a high peak of magnetic susceptibility. A fourth tsunami layer

444 of medium to fine pale yellow sand, with broken shells fragments, is identified in section 2

445 (Fig. S2 – 12 b) at 151 cm depth. It is characterized by and poor sorting, high peak of

446 magnetic susceptibility, a large amount of organic matter (> 5.5) and high amount of gypsum.

447 Five samples were collected for dating in core 12. In core section 1, the first sample is

448 a gastropod found at 44 cm depth that gives an age of 3367-3366 BC. The second sample is a

449 shell found at 108 cm depth and shows an age of 3097-3950 BC (Table 2 b). The third sample

450 is a gastropod found at 114 cm depth dated at 3331-4050 BC. The fourth and fifth samples in

451 core section 2,sample are gastropod shells found at 117 cm and 135 cm depth with calibrated

452 age 39560- 40811 BC and 3365-4071 BC, respectively (Table 2 b). The fourth sample is off

453 sequence with respect to the other samples and may result from sediment transport and

454 reworking due to high energy tsunami waves. The other samples are in sequence from 4071 to

455 2457 BC age, comparable to the sedimentary succession of core 11.

456 ***Results:*** The sedimentary deposits in the El Alamein lagoon also result from

457 intercalated high-energy marine deposits into low energy marine and alluvial deposits with

458 reworked sedimentation. A first observation in almost all cores is the existence of the white

459   sand layer with broken shells of marine origin located ~ 10 cm to 75 cm depth in El Alamein

460   site, and the identified three to four tsunami layers. The tsunami layers and their catastrophic

461   content are identified in photography and X-rays, magnetic susceptibility, organic/mineral

462   content and by the existence of mixed coarse and fine sand with broken marine shells. A main

463   difficulty, however, is the age determination of the tsunami layers due to the mixed

464   radiocarbon dates that can be ranged in old and young ages, between 50000 year BP - 13430

465   year BP, and 5065 year BP - 125 year BP, respectively, in all cores.

466   As the sedimentary units in the 1 m to 2.6 m depth cores result from young deposition

467   processes with high-energy marine units intercalated into low energy marine and alluvial

468   deposits, we consider the radiocarbon dating older than 13430 year BP as due to sedimentary

469   units that include reworked material. Considering that the succession of 2.6 m uppermost

470   deposits and related stratigraphic chronology are comparable in all cores in the El Alamein

471   lagoon, we select the radiocarbon dates younger than 5500 year BP as representative of the

472   recent sedimentary units that include tsunami layers. Using the radiocarbon dating of samples

473   and related selected young ages, the sedimentary sequence of catastrophic layers and their

474   ages obtained from the Bayesian simulation (Oxcal 4.2.4; Bronk-Ramsey, 2013) allow a

475   correlation with the AD 365, AD 1303 and AD 1870 tsunamigenic earthquakes of the east

476   Mediterranean Sea (Fig. 6). In addition, a fourth tsunami layer can be identified between 1126

477   BC and 1434 BC.

478

479   **6. Summary of results from trenching and coring**

480   The cores and trenches in both Kefr Saber and El Alamein sites show three main

481   layers characterized by fine and coarse sand mixed with broken shell fragments that indicate

482   the occurrence of high energy and catastrophic sedimentary deposits in the coastal lagoon

483   environment (Figs. 2 a, b, and c, and Fig. 3). Although the two studied sites are ~200 km

484   apart, a white sandy layer with broken shells is found in all trenches (see Fig. 3 and

485   supplemental material S1 a, b, c, d, e) and cores (except for core 5, see Figs. 5 a and b, and

486   supplemental material in Fig. S2 – 1 to 12). The recurrent white sandy deposits in trenches

487   and cores are well visible coarse sand units mixed with gravel and broken shells that become

488   fine landward (see trench P4, Fig. 3) or disappear when distant from the shore (core 5, Fig. S2

489   – 5). All these signatures with only three layers in the ~ 2 m thick sedimentary units indicate

490   that this layer suggests tsunami deposits rather than storm.

491   In most cores (Figures. 5 a and b, and supplemental material Fig. S2 – (1 - 12), the

492   first tsunami layer is ~7.5-cm-thick at ~19 cm-depth and is made of poorly sorted white sandy

493   deposits with broken gastropods and lamellibranch (shell) fossils. This layer is characterized

494   by bi-modal grain size distribution with high value of organic matter and peak of magnetic

495   susceptibility with a rich content in carbonates and quartz. The presence of goethite and pyrite

496   heavy minerals was found in the cores at the base of layer 1, which contains rip up clasts from

497   underlying sediments. The second layer is ~13-cm-thick at ~32.5-cm-depth characterized by

498   white sandy deposits intercalated with coarse brown sand horizontal lamination, very poor

499   sorting of sediments, rich in organic matter and with a high peak of magnetic susceptibility.

500   The pebbles also are found at the base of this layer which reflects a loading structure. A

501   considerable amount of heavy minerals like Goethite and Pyrite can be found in this layer.

502   The third layer is ~25-cm-thick at ~89-cm-depth is made of grey sandy clay, with a high peak

503   of magnetic susceptibility, laminations at the bottom of deposits, vertically aligned

504   gastropods, broken shells fragments, and rich in total organic matter. In all three layers, the

505   poorly sorted sediments and organic content greater than 5 mark the high energy deposits and

506   tsunami records (Folk, 1968). All these characteristics at the El Alamein site lead us to

507   interpret the three sedimentary layers as tsunami deposits.

508   In a synthesis of all dated units in trenches and cores in Figures 4 and 6, the

509   sedimentary succession of low energy marine and alluvial deposits intercalated with high-

510   energy deposits provides evidence for the identification of four tsunami deposits at Kefr Saber

511   and El Alamein sites. In the case of Kefr Saber trenches, the dating of charcoal fragments

512   allows the bracket of a tsunami event with a simulated age between AD 137 and AD 422,

513   which includes the AD 365 western Crete earthquake (Figs. 4 and Table 2 a). The dating of

514   sedimentary units at the El Alamein site turned out to be more complex due to the reworked

515   sedimentation with significant mix of old (> 13000 year BP) and young ages (< 5500 year BP;

516   Table 2 b). Using the latter ages, the radiocarbon dating (including the Oxcal Bayesian

517   analysis) of shells, bone and charcoals fragments at El Alamein site (Fig. 6) result in a

518   sequence of ages that allow the bracket of an event W between 1434 BC and 1126 BC, and

519   event X between AD 48 and AD 715, and event Y between AD 1168 and AD 1689, and an

520   event Z between AD 1805 and AD 1935 (Figure 6). The three most recent simulated dates of

521   tsunami events X, Y and Z correlate with the seismogenic tsunamis of AD 365, AD 1303 and

522   AD 1870 reported in catalogues (Table 1).

523

524   **Discussions and Conclusions**

525   The identification of tsunami deposits within the stratigraphic layers and results of

526   radiocarbon dating allow the chronological simulation of the three most recent tsunami events

527   (Figs. 4 and 5). The historical seismicity catalogue of the Eastern Mediterranean reported two

528   significant tsunamigenic seismic events of the Hellenic subduction zone that affected the

529   Mediterranean coast of Egypt: 1) The 21 July 365 earthquake (Mw 8.3 – 8.5; Stiros and

530   Drakos, 2006; Shaw et al., 2008), 2) the 8 August 1303 earthquake (Mw 7.8 – 8.0; Abu Al

531   Fida, 1907; Ambraseys, 2009). A third tsunami event is also reported during the 24 June 1870

532   earthquake (Mw 7 - 7.5), but despite some debates on its occurrence, the inundation of the

533   Alexandria harbour leaves no alternative on the tsunami waves on the Egyptian coastline (see

534   section 2). Hence, the dating of the three high energy sedimentary layers deposited along the

535   Egyptian coastline at Kefr Saber and El Alamein sites correlate with the historically recorded

536   seismogenic tsunamis of the Hellenic subduction zone.

537   In our study, the distinction of tsunami sedimentary records from storm deposits is

538   based on: 1) The record of the small number (3 to 4) layers while storm deposits controlled by

539   seasonal climatic catastrophic events should have been more frequent. 2) The existence of

540   white sand sheet layers with broken shells at two sites (Kefer Saber and El Alamein) located

541   ~200 km apart, bearing comparable age, structure and texture. 3) The existence of organic

542   rich clasts in sand sheets of some cores (Shi et al., 1995; Gelfenbaum and Jaffe, 2003) which

543   indicates a catastrophic event with sufficient energy to break and erode the coastal barrier

544   made of the shoreline rocky headlands, organic sediments and coastal dunes before reaching

545   the lagoons. 4) The bimodal distribution of the grain size of sandy sedimentary units that

546   include a large proportion of broken shell comparable to that of tsunami deposits (Goff et al.,

547   2001, 2004). 5) The correlation between the simulated ages of tsunami layers from the

548   radiocarbon dating and the large historical tsunamigenic earthquakes of the eastern

549   Mediterranean (Figs. 4 and 6). 6) The consistent depth of tsunami layers in cores of the El

550   Alamein site (Fig. 7).

551   The lagoon sedimentary environment is a natural site of mixed and reworked marine

552   and continental deposits that may explain the mixed radiocarbon dates (Tables 2 a and b).

553   Indeed, by considering the mixed sedimentation of reworked deposits intercalated with new

554   units, our selection of samples younger than 2000 year BP at Kefr Saber, and younger than

555   5500 year BP at El Alamein allowed us to distinguish between old and new isotopic dating

556   and infer a consistent chronology of tsunami deposits. For instance at the El Alamein lagoon,

557   the clear separation between old (50000 year BP to13430 year BP) and young (5065 year BP -

558   125 year BP) radiocarbon dating, with no intermediate dates of sedimentation, confirms the

559   different origin and processes of deposition. The radiocarbon dating indicate that the white

560   sand and coarse mixed layers represent deposits that may result from tsunamis events in 365,

561   1303 and 1870 (see Table 1). The first two events are large earthquakes with Mw≥8 with well

562   documented tsunami waves in the historical sources. The evidence of the 365 tsunami seems

563   to be widely recorded through widespread massive turbidities of the eastern Mediterranean

564   region (Stanley et al., 2006; Polonia et al., 2016). The four main catastrophic layers in

565   trenches and cores have physical and chemical characteristics that correlate with high energy

566   environmental conditions of tsunami deposits. The four high magnetic susceptibility peaks of

567   the four deposits also correlate with the high value of organic matter and carbonates.

568   The record of past tsunami deposits is favored by the low topography and platform

569   geomorphology along the Egyptian Mediterranean coastline. The coastal environment with

570   similar lagoons and dunes with large areas with relatively flat morphology allowed the

571   deposits of catastrophic marine deposits intercalated within alluvial deposits. The lagoon

572   shapes elongated along the shoreline at Kefr Saber and El Alamein sites explain the similarity

573   between the sedimentary units and the tsunami deposits. The correlation between the core

574   deposits at El Alamein and trench deposits at Kefr Saber are marked by the dating of tsunami

575   deposits and the correspondence with the AD 365 earthquake. The succession of sudden high-

576   energy deposits with low energy and slow sedimentation may include reworked units with a

577   disturbance in their chronological succession. In comparison with the trench results of Kefr

578   Saber, the sedimentary sequence from cores at El Alamein reveals mixed old and young dates

579   likely due to the sedimentary environment with large lagoon and nearby topography with the

580   supply of colluvial and alluvial deposits. Despite the richness of charcoal fragments, bones

581   and shells in the sedimentary record, the reworking implies significant out of sequence dating

582   and large uncertainties (see Table 2 b, among 30 samples 12 dated samples are > 30 ka).

583   Although the results of dated shells may be suspicious (due to the unclosed mineralogical

584   system), their reliability is tested with the comparison of nearby radiocarbon dating.

585   The size of past tsunamis can be compared with the thickness of catastrophic

586   sedimentary units in trenches of Kefr Saber and core units of the El Alamein site. It appears

587   that the tsunami deposits of the AD 365 tsunamigenic earthquake have a larger thickness at

588   Kefr Saber site than at the El Alamein site. In contrast, the thickness of sedimentary layers of

589   the AD 1303 and AD 1870 are thicker at the El Alamein site. These observations can be

590   justified by the proximity of the tsunamigenic source in western Crete of the AD 365

591   earthquake with respect to the Kefr Saber paleotsunami site, and the proximity of the AD

592   1303 and AD 1870 seismic sources in the east Hellenic Arc with regards to the El Alamein

593   paleotsunami site. Our results on the identification of past tsunamis and their repetition along

594   the coastlines in Egypt and North Africa are decisive for the tsunami wave propagation and

595   hazard models in the East Mediterranean Sea (Salama, 2017).

596

597   **Author contribution**:

598   A. Salama and M. Meghraoui wrote the text manuscript; A. Salama did the analysis of trench

599   and core deposits, and interpretation of tsunami events; M. Meghraoui, M. El Gabry, H.

600   Hussein and I. Korrat did the earthquake data analysis and interpretation; all authors

601   contributed to the field investigations.

602

603   **Competing interests:** The authors declare that they have no conflict of interest.

604

605   **Supplement:**

606   Supplementary data associated with this manuscript are:

607   ▪ Figures S1 a, b,c, d and e of five trench logs of Kefr Saber site (trench P4 as Fig. 3).

608 ▪ Figure S2 – 1 (section 2) to 10 of core descriptions of El Alamein site (cores 1 and 9 as

609   Figs a and b).

610

611

612 **Acknowledgments**

613 We are grateful to Prof. Hatem Odah and NRIAG administration, and staff for their keen

614 efforts and help during the development of this work. We are grateful to the North African

615 Group for Earthquake and Tsunami studies (NAGET) and Drs. Assia Harbi, Adel Samy,

616 Hany Hassen, Mohamed Maklad, Mohamed Sayed for support and discussions. We are

617 grateful to the "*Centre d'Etudes Alexandrine*" for the lending of the COBRA instrument for

618 coring. We address our special thanks to the Egyptian Armed Forces for issuing permissions

619 and their support during field work. This research programme is conducted with the funding

620 support of the ASTARTE EC project (Assessment, Strategy And Risk Reduction for

621 Tsunamis in Europe - FP7-ENV2013 6.4-3, Grant 603839), the French-Egyptian IMHOTEP

622 project, and the Academy of Scientific Research and Technology of Egypt.

623

624

625 **References**

626 Abbas, M.S., El-Morsy, M.H., Shahba, M.A. and Moursy, F.I.,: Ecological studies in coastal

627   sand dune rangelands in the North-West of Egypt, Meeting of the Sub-network on

628   Mediterranean Forage Resources of the FAO-CIHEAM Inter-regional Cooperative

629   Research and Development Network on Pastures and Fodder Crops, Spai: , 389–393,

630   2008.

631 Abu al-Fida Ismail Ibn Hamwi (born 1273 – died 1331). : The Concise History of Humanity

632   or Chronicles (in Arabic *'Tarikhu 'al-Mukhtasar fi Akhbar al-Bashar'* in 1329). Al-

633   Husayniyah Press, Cairo, 2 volumes , 1112 p., 1907.

634 Ambraseys, N.N., Melville, C.P. and Adam, R.D.: The seismicity of Egypt, Arabia and Red

635   Sea: A Historical Review, Cambridge University Press, 181 p., 1994.

636 Ambraseys, N.: Earthquakes in the Mediterranean and Middle East: A Multidisciplinary
637   Study of Seismicity up to 1900, Cambridge University Press, 947 p., 2009.

638 Atwater, B.: Evidence for great holocene earthquakes along the outer coast of Washington
639   state, Science, 236, 942 – 944, 1987.

640 Babu, N., Suresh Babu D.S. and Mohan Das P.N.: Impact of tsunami on texture and
641   mineralogy of a major placer deposit in southwest coast of India, Environmental Geology
642   52, 71–80, 2007.

643 Ben Menahem, A.: Earthquake catalogue for the Middle East (92 B.C. to 1980 A.D.)
644   Bollettino di Geofisica Teorica ed Applicata, 2I, 245-310, 1979.

645 Ben Menahem, A.: Four thousand years of seismicity along the Dead Sea rift, Journal of
646   Geophysical Research, 96, 195–216, 1991.

647 Bronk-Ramsey, C.: Bayesian analysis of Radiocarbon, Radiocarbon, 51(1), 337–360, 2009.
648
649 Bronk-Ramsey, C., & Lee S.: Recent and Planned Developments of the Program OxCal,
650   Radiocarbon, 55(2-3), 720-730, 2013.

651 Coumbary, A. : Sur le tremblement de terre du 24 juin 1870, Nouvelles Météorologiques
652   Paris, 3, 200-201, 1870.

653 CMT catalogue: Centroid Moment Tensor catalogue of Harvard,
654   http://www.seismology.harvard.edusearch.html, 2018.

655 De Martini, P.M., Barbano, M.S., Pantosti, D., Smedile, A., Pirrotta, C., Del Carlo, P., and
656   Pinzi, S.: Geological evidence for paleotsunamis along eastern Sicily (Italy): An
657   overview: Natural Hazards and Earth System Sciences, 12 (8), 2569–2580, 2012.

658 Donato, S.V., E.G. Reinhardt, J.I.Boyce, R. Rothaus & T. Vosmer.: Identifying tsunami
659   deposits using bivalve shell taphonomy, Geology, 36 (3), 199-202, 2008.

660 El-Sayed, A., Korrat, I., and Hussein, H. M.: Seismicity and seismic hazard in Alexandria
661   (Egypt) and its surroundings, Pure and Applied Geophysics, 161, 1003–1019, 2004.

662 Folk, R.L.: Petrology of sedimentary rocks, in Austin, Texas, HemphilPs Book Store, 182 p.,
663   1968.

664 Font, E., C. Nascimento, Baptista M.A. & Silva P.F.: Identification of tsunami induced
665   deposits using numerical modelling and rock magnetism techniques: A study case of the
666   1755 Lisbon tsunami in Algarve, Portugal, Physics of the Earth and Planets Interiors,
667   182, 187−198, 2010

668 Frihy, O.E., Deabes, E. a., and El Gindy, A. a.: Wave Climate and Nearshore Processes on the
669   Mediterranean Coast of Egypt: Journal of Coastal Research, 261, 103–112, 2010.

Galanopoulos, A.G.: The seismic sea-wave of 9 Iouliou 1956, Praktika Academy Athens, 32, 90–101, 1957.

Goff, J., Chague-Goff, C., and Nichol, S.: Palaeotsunami deposits: A New Zealand perspective, Sedimentary Geology, 143 (1–6), 2001.

Goff, J. R., McFadgen, B. G., and Chagué-Goff, C.: Sedimentary differences between the 2002 Easter storm and the 15th century Okoropunga tsunami, southeastern North Island, New Zealand, Marine Geology, 204, 235–250, 2004.

Goff J, Dudley WC, de Maintenon MJ, Cain G, Coney JP.: The largest local tsunami in 20th century Hawaii, Marine Geology 226, 65–79, 2006

Goff, J.R., Lane, E., Arnold, J.: The tsunami geomorphology of coastal dunes, Natural Hazards Earth System Sciences, 9 (3), 847–854, 2009.

Goff, J., Chagué-Goff, C., Nichol, S., Jaffe, B., Dominey-Howes, D.: Progress in palaeotsunami research, Sedimentary Geology, 243, 70–88, 2012.

Guidoboni, E., Comastri, A. and Traina G.: Catalogue of Ancient Earthquakes in the Mediterranean area up to the 10th century, INGV-SGA, Bologna, 504 p., 1994.

Guidoboni, E., and A. Comastri : Catalogue of earthquakes and tsunamis in the Mediterranean area from the 11th to the 15th century, INGV-SGA, Bologna, 1037 p., 2005.

Gelfenbaum, G., and B. Jaffe .: Erosion and sedimentation from the 17 July, 1998 Papua New Guinea tsunami, Pure and Applied Geophysics, 160, 1969–1999, 2003.

Hassouba, A.B.H.: Quaternary Sediments from the Coastal Plain of Northwestern Egypt (from Alexandria to Elomayid), Carbonates and Evaporites, 10 (1), 8–44, 1995.

Hall AM, Hansom JD, Williams DM, and Jarvis J.: Distribution, geomorphology and lithofacies of cliff- top storm deposits: examples from the high-energy coasts of Scotland and Ireland. Marine Geology, 232, 131–155, 2006.

Hamouda, A.Z.: Numerical computations of 1303 tsunamigenic propagation towards Alexandria, Egyptian coast, Journal African Earth Science, 44, 37-44, 2006.

Hamouda, A.Z.: A reanalysis of the AD 365 tsunami impact along the Egyptian Mediterranean coast, Acta Geophysica, 58 (4), 687–704, 2009.

Jusseret, S. and Sintubin, M., Minoan Earthquakes: Breaking the Myth through Interdisciplinarity, Studies in Archaeological Sciences, Leuven University Press, 440 pp., 2017

Maamoun, M., Megahed, A. and Allam, A.: Seismicity of Egypt, NRIAG Bulletin, IV (B), 109–160, 1984.

703   Maramai, A., Brizuela, B., Graziani, L. : The Euro- Mediterranean tsunami catalogue. Annals
704   of Geophysics, 57 (4), 1-26, 2014.

705   Marriner, N., Kaniewski, D., Morhange, C., Flaux, C., Giaime, M., Vacchi, M., and Goff, J.:
706   Tsunamis in the geological record, Making waves with a cautionary tale from the
707   Mediterranean, Science Advances, 1-12, 2017.

708   Malik, J.N., Banerjee, C., Khan, A., Johnson, F.C., Shishikura, M., Satake, K., and Singhvi,
709   A.K.: Stratigraphic evidence for earthquakes and tsunamis on the west coast of South
710   Andaman Island, India during the past 1000years, Tectonophysics, 661, 49–65, 2015.

711   Matsumoto, D., H. Naruse, S. Fujino, A.Surphawajruksakul, T., Jarupongsakul, N., Sakakura
712   & M. Murayama : Truncated flame structures within a deposit of the Indian Ocean
713   Tsunami: evidence of syn-sedimentary deformation, Sedimentology, 55, .1559-1570,
714   2008.

715   Maouche, S., Morhange, C. and Meghraoui, M.: Large boulder accumulation on the Algerian
716   coast evidence tsunami events in the western Mediterranean, Marine Geology, 262 (1),
717   96-104, 2009.

718   Morhange, C., Marriner, N., Pirazzoli, P.A.: Evidence of Late-Holocene tsunami events from
719   Lebanon, Z. Geomorphology, 46, 81–95, 2006.

720   Nanayama, F., Satake, K., Furukawa, R., Shimokawa, K., Atwater, B.F., Shigeno, K., and
721   Yamaki, S.: Unusually large earthquakes inferred from tsunami deposits along the Kuril
722   trench, Nature, 424 (6949), 660–663, 2003.

723   Paris, R., F., Lavigne, P.,Wassmer, and J.,Sartohadi : Coastal sedimentation associated with
724   the December 26, 2004 tsunami in Lhok Nga, West Banda Aceh (Sumatra, Indonesia).
725   Marine Geology, 238, 93–106, 2007.

726   Papadopoulos, G.A., E. Daskalaki, A. Fokaefs and N. Giraleas.: Tsunami hazard in the
727   Eastern Mediterranean Sea: strong earthquakes and tsunamis in the West Hellenic Arc
728   and Trench System, Journal Earthquake and Tsunami, 4 (3), 145-179, 2010.

729   Papadopoulos, G. A., Gràcia, E., Urgeles, R., Sallares, V., De Martini, P. M., Pantosti, D.,
730   González, M., Yalciner, A. C., Mascle, J., Sakellariou, D., et al.: Historical and pre-
731   historical tsunamis in the Mediterranean and its connected seas: Geological signatures,
732   generation mechanisms and coastal impacts, Marine Geology, 354, 81–109, 2014.

733   Polonia, A., Vaiani, S.C., de Lange, G.J.: Did the A.D. 365 Crete earthquake/tsunami trigger
734   synchronous giant turbidity currents in the Mediterranean Sea?, Geology, 44, 191-194,
735   2016.

736   Poirier, J. P. and Taher, M.A.: Historical Seismicity in the near and Middle East, North
737   Africa, and Spain from Arabic Documents (VIIth- XVIIIth Century). Bulletin Society
738   Seismology American, 70 (6), 2185–2201, 1980.

739   Reimer PJ, and 24 co-authors.: Selection an treatment of data for radiocarbon calibration: an
740   update to the International Calibration (IntCal) criteria, Radiocarbon, 55 (4), 1869-1887,
741   2013.

742   Salama, A.: Active tectonics and Paleo-tsunami records of the Northern Coast of Egypt, Ph.D
743   thesis dissertation, University of Strasbourg (France), 429 pp., 2017.

744   Salamon, A., Rockwell, T., Ward, S. N., Guidoboni, E. & Comastri, A.: Tsunami hazard
745   evaluation of the Eastern Mediterranean: Historical analysis and selected
746   modeling, Bulletin of the Seismological Society America, 97, 705–724, 2007.

747   Schmidt, J.F.: Studien ueber Erdbeben. 1-136, 316-360, Leipzig, 1879.

748   Srinivasalu S, Rajeshwara-Rao N, Thangadurai N, Jonathan M P, Roy P D, Rammohan V and
749   Saravanan P., 2009. Characteristics of 2004 tsunami deposits of northern Tamil Nadu
750   coast, India; Boletin de la Sociedad Geologica Mexicana, 61, 111–118, 2009.

751   Shah-Hosseini, M., Saleem, A., Mahmoud, A. and Morhange, C.: Coastal boulder deposits
752   attesting to large wave impacts on the Mediterranean coast of Egypt, Natural Hazards, 83
753   (2), 849-865, 2016.

754   Shaw, B., Ambraseys, N. N., England, P.C., Floyd, M., Gorman, G.J., Higham, T.F.G.,
755   Jackson, J., Nocquet, J-M., Pain, C. C., and Piggott, M. D.: Eastern Mediterranean
756   tectonics and tsunami hazard inferred from the AD 365 earthquake, Nature Geoscience, 1
757   (April), 268–276, 2008.

758   Shi, S., Dawson, A.G. & Smith, D.E. Coastal sedimentation associated with the December
759   12th, 1992 tsunami in Flores, Indonesia, Pure and Applied Geophysics, 144, 525-536,
760   1995.

761   Soloviev, S.L., Solovieva, O.N., Go, C.N., Kim, K.S., and Shchetnikov, N.A.: Tsunamis in
762   the Mediterranean Sea 2000 B.C.-2000 A.D., Advances in Natural and. Technological
763   Hazards Research, Kluwer Academic Publishers, Dordrecht,. Netherlands, 13, 237 p.,
764   2000.

765   Stanley, J.D. – Bernasconi, M.P.: Holocene depositional patterns and evolution in
766   Alexandria's eastern harbor, Egypt, Journal of Coastal Research, 22 (2), 283-297, 2006.

767   Stiros, S. C.: The AD 365 Crete Earthquake and Possible Seismic Clustering During the
768   Fourth to Sixth Centuries AD in the Eastern Mediterranean: A Review of Historical and
769   Archaeological Data, Journal of Structural Geology, 23, 545–562, 2001.

770 Stiros, S., and Drakos, A.: A fault model for the tsunami-associated magnitude >8.5 Eastern
771   Mediterranean, AD 365 earthquake, Zeitschriftfür Geomorphologie, 146, 125–137,
772   2006.

773 Spiske, M., Böcz, Z., and Bahlburg, H.: The role of porosity in discriminating between
774   tsunami and hurricane emplacement of boulders—a case study from the Lesser Antilles,
775   southern Caribbean, Earth Planet. Science Letters, 268, 384–396, 2008.

776 Switzer, A. D. and Jones, B. G.: Large scale washover sedimentation in a freshwater lagoon
777   from the southeast Australian coast: sea level change, tsunami or exceptionally large
778   storm?, The Holocene, 18 (5), 787-803, 2008.

779 Szczucinski, W., Chaimanee, N., Niedzielski, P., Rachlewicz, G., Saisuttichai, D., Tepsuwan,
780   T., Lorene, S. and Siepak, J.: Environmental and geological impacts of the 26
781   December 2004 Tsunami in coastal zone of Thailand- Overveiw of short and long term
782   effects. In: Polish Journal of Environmental studies, 15 (5), 793-810, 2006.

783 Taymaz, T., Westaway, R., and Reilinger, R.: Active faulting and crustal deformation in the
784   Eastern Mediterranean region, Tectonophysics, 391, 1–9, 2004.

785 Tinti, S., Maramai, A. and Graziani, L.: A New Version of the European Tsunami Catalogue:
786   Updating and Revision, Natural Hazards and Earth System Sciences, 1, 255-262, 2001.

787 Tinti, S., Manucci, A., Pagnoni, G., Armigliato, A., and Zaniboni, F.: The 30 December 2002
788   landslide-induced tsunamis in Stromboli: sequence of the events reconstructed from the
789   eyewitness accounts, Natural Hazards and Earth System Science, 5 (6), 763–775, 2005.

790 Tuttle, M.P., Ruffman, A., Anderson, T., and Jeter, H.: Distinguishing tsunami from storm
791   deposits in eastern North America: the 1929 Grand Banks tsunami versus the 1991
792   Halloween storm, Seismological Research letters, 75, 117-31, 2004.

793 Yalciner, A., Zaytsev, A., Aytore, B., Insel, I., Heidarzadeh, M., Kian, R., and Imamura, F.: A
794   Possible Submarine Landslide and Associated Tsunami at the Northwest Nile Delta,
795   Mediterranean Sea: Oceanography, 27, (2), 68–75, 2014.

796

797

Figure captions

Figure1: Seismicity (instrumental with M> 5.5) and main tectonic framework of the east Mediterranean regions. Black boxes indicate the paleoseismic sites of Kefr Saber and El Alamein east of the Nile delta. The major historical earthquakes (Table 1) AD 365 (Mw 8 – 8.5), AD 1303 (Mw ~8) and AD 1870 (Mw ~7.5) are located along the Hellenic subduction zone according to Guidoboni et al. (1994), Stiros (2001); Ambraseys (2009); Papadopoulos et al. (2014) and Jusseret and Sintubin (2017). Focal mechanisms are CMT-Harvard (last accessed January 2018), and the background topography is from GEBCO.

Figure 2: Location of trenches and core sites at (a) Kafr Saber, (b) El Alamein (see also Figure 1), and (c) Dune ridge and a lagoon south of the Mediterranean Sea as a selected site for coring and trenching.

Figure 3: a) Trench dimensions at Kefr Saber, and (b) description of sedimentary layers of trench P 4 with carbon dating sampling (yellow flag); the horizontal ruler indicates 20 cm scale.

Figure 4: Radiocarbon dating calibrated with probability density function (pdf) using Oxcal version 4.2 (Bronk-Ramsey, 2013) and chronology of sedimentary layers and tsunami record of trenches at Kefr Saber. The dating characteristics are in Table 2 a. The Bayesian dating simulation of the white sandy unit in Fig. 3 b can be correlated with the 365 AD tsunami event.

821 Figure 5: a) Core 1 description with X-ray scanning, lithology log, magnetic susceptibility,

822 mean grain size, sediment sorting, total organic and inorganic matter and bulk mineralogy.

823 The arrows show the high values of each measurement that may correlate with tsunami

824 deposits.

825 b) Core 9 photography, X-ray scanning, lithology log, magnetic susceptibility, mean grain

826 size, sediment sorting, total organic and inorganic matter and bulk mineralogy. The arrows

827 show the high values of each measurement that may correlate with tsunami deposits.

828 (Similar illustrations of cores 2 to 12 are in supplemental materials).

829

830 Figure 6: Radiocarbon dating calibrated with probability density function (pdf) using Oxcal

831 version 4.2 (Bronk-Ramsey, 2013) and chronology of sedimentary layers with dated tsunami

832 records at El Alamein. The dating characteristics are in Table 2 b. Black pdfs refer to the

833 dated samples and red pdfs are simulated dating of the four tsunami records. Three

834 sedimentary records are correlated with the historical earthquake and tsunami catalogue of the

835 eastern Mediterranean (See also Table 1).

836

837 Figure 7: Depth distribution of tsunami layers in cores at the El Alamein site (see also core

838 locations in Fig. 2 b). The depth correlation of paleotsunami layers indicates the consistent

839 succession of deposits in the lagoon. Deposits of layers 1, 2 and 3 are related with tsunami

840 events 1870 AD, 1303 AD and 365 AD of the East Mediterranean Sea (see also Fig. 6 and

841 Table 1). Layer 4 corresponds to tsunami event 1491 – 1951 BC and is not reported in

842 tsunami catalogues.

843

844

845

846

847 **Table captions**

848 Table 1: Major earthquakes of the eastern Mediterranean with tsunami wave reports in

849 northern Egypt. Estimated magnitudes are given in Mw when calculated and in M when

850 estimated.

851

852 Table 2 a: Radiocarbon dating samples and calibrated ages at Kefr Saber site using OxCal

853 v4.2.4 (Bronk-Ramsey, 2013).

854

855 Table 2 b: Radiocarbon dating samples and calibrated ages in El Alamein site using OxCal

856 v4.2.4 (Bronk-Ramsey, 2013)

857

858
859
860
861

862   Table 1: Major earthquakes of the eastern Mediterranean with tsunami wave reports in
863   northern Egypt. Estimated magnitudes are given in Mw when calculated and in M when
864   estimated.
865
866

Date	Epicentre	Estimated Magnitude	Comment	Reference
21 July 365	Western Crete	8.3 – 8.5 (M_w)	Tsunami northern Egypt	Stiros and Drakos, 2006; Shaw et al., 2008, Hamouda 2009
18 Jan. 746	Dead Sea Fault	7.5 (M)	Tsunami eastern Medit.	Ambraseys, 1962
881 - 882	Palestine	?	Tsunami in Alexandria & Palestine	Galanopoulos A., 1957
4 Jan. 1033	Jordan Valley Fault	7.4 (M)	Tsunami northern Egypt	Ambraseys, 1962
18 Jan. 1068	Northern Lebanon	6.9 (M)	Waves in Lebanon Until northern Egypt	Ambraseys, 1962, Soloviev et al., 2000
8 Aug. 1303	Karpathos & Rhodos islands	8 (M)	>8-m-high wave in Alexandria	Abu al-Fida1329, Ambraseys 2009, Hamouda 2006
24 June 1870	Hellenic Arc	M_L 7.2	Inundation in Alexandria harbour	Ben-Menahem, 1979, Soloviev et al., 2000

867
868

869

870

871

872 Table 2 a: Radiocarbon dating samples and calibrated age at Kefr Saber site using OxCal
873 v4.2.4 (Bronk-Ramsey, 2013).
874

No.	Sample name	Laboratory Name	Type of samples	Depth (m)	Date BP	Calibrated. date
1	KSB2S2	Poznan	Dendropoma	Boulder	890 ± 30 BP	940 - 1446 AD
2	TSU P1 S07B	Poznan	Charcoal	35	110.14±0.3 BP	Modern
3	TSU P1 S09B	CIRAM	Charcoal	53	40560 BP	39000-38250 BC
4	TSU P3S2	CIRAM	charcoal	73	2000 BP	50-70 AD
5	TSU P3S3	CIRAM	Charcoal	100	6240 BP	5300 – 5070 BC
6	TSU P3 S2	Poznan	Charcoal	72	1075 ± 30 BP	890 – 1020 AD
7	TSU P4 S2	CIRAM	Charcoal	61	Modern	-
8	TSU P4 S3	CIRAM	Charcoal	40	Modern	-
9	TSU P4 S4	CIRAM	Charcoal	15	Modern	-
10	TSU P4 S5	Poznan	Charcoal	60	15490 ± 70 BP	17200 – 15900 BC
11	TSU P4 S6	Poznan	Charcoal	25	101.42 ± 0.68 BP	1700 – 1920 AD
12	TSU P5S1	Poznan	Charcoal	12	2145 ± 30 BP	360 – 50BC
13	TSU P5S2	Poznan	Charcoal	37	4560 ± 300 BP	4000 – 2400 BC
14	TSU P5S3	Poznan	Charcoal	17	2060 ± 35 BP	180 – 30 AD
15	TSU P5S4	Poznan	Charcoal	33	2590 ± 140 BP	1050 – 350 BC

875
876 ▪ CIRAM Lab. science for art cultural heritage ,archeology department http://www.ciram-
877   art.com/en/archaeology.html
878 ▪ Poznan Lab. Poznan Radiocarbon Laboratory, Poland, email: c.fourteen@radiocarbon.pl
879   http://radiocarbon.pl/index.php?lang=en.
880 ▪ Beta Analytic radiocarbon dating, Miami, Florida, USA http://www.radiocarbon.com/, e-mail:
881   lab@radiocarbon.com
882
883

884
885
886
887
888
889
890

891 Table 2 b: Radiocarbon dating samples and calibrated date in El Alamein site using OxCal
892 v4.2.4 (Bronk-Ramsey, 2013)
893

No.	Sample name	Laboratory Name	Type of samples	Depth (m)	Date BP	Calibrated date (2σ)
a	AL1 S1 (test pit)	CIRAM	charcoal	25	130±20	1680-1908 AD
b	AL1 S2 (test pit)	CIRAM	charcoal	56	190±20	1661-1931 AD
1	core 1/1sa1	Poznan	charcoal	40	13430±60	13985-14415 BC
2	core 1/1sa2	Poznan	Bone	50	1540±60	403-634 AD
3	core2/1sa4	Poznan	gastropods	77	35500±500	34362-36931 BC
4	core2/1sa6	Poznan	gastropods	75	32000±360	32971-34681 BC
5	core 3/1sa1	Poznan	shell	45	33500±600	34218- 37224 BC
6	core 3/1sa2	Poznan	bivalve	37	45000±2000	43618 BC
7	core 4/1sa1	Poznan	shell	28	31840±350	32887-34447BC
9	core 6/2 sa1	Poznan	charcoal	80	125±30	<1620 AD
10	core 6/1 sa6	Poznan	gastropod	45	34000±400	35002-37441 BC
11	core 6/1sa9	Poznan	coral	60	50000±4000	42776-69225 BC
12	core 7/1sa1	Poznan	shell	17	3000±30	293-1113 BC
12	core 9/1sa1	Poznan	gastropod	24	3320±30	1052-1888 BC
13	core 9/1sa5	Poznan	bivalve	55	40000±800	40521-43169 BC
14	core 10/1sa2	Poznan	bone	70	42000±1300	41256-46581 BC
15	core10/1sa3	Poznan	shells	20	4515 ±30	2623-3521 BC
16	core11/2sa1	Beta analytic	roots	139	4810±30	2666 - 2817 BC
17	core 11/1sa1	Beta analytic	gastropod	20	5230±30	3638-4328 BC
18	core11/2Sa4	Poznan	gastropod +shell	116	4500±35	2619-3386 BC
19	core11/2sa6	Poznan	gastropod	126	4405±35	2477-3368 BC
20	core11/2 sa11	Beta analytic	shells	152	32500±500	33294-36120 BC
21	core 11/2sa2	Beta analytic	shell	62	16900±60	17869-18741 BC
22	core 11-2	Beta analytic	charcoal	180	5020±30	3710-3943 BC
23	core 11 2_5	Poznan	gastropod	121	4360±40	2457-3366 BC
24	core 12/1 sa1	Poznan	gastropod	44	5065±30	3367-4072 BC
25	core 12/2sa1	Beta analytic	gastropod	108	4885±35	3097-3950 BC
26	core 12/2sa2	Poznan	gastropod	114	5000±35	3331-4050 BC
27	core 12/2 sa3	Beta analytic	broken shell	117	37940±420	39560 -40811 BC
28	core 12/2sa4	Beta analytic	roots	135	5060±30	3365-4071 BC

894
895 ▪ CIRAM Lab. science for art cultural heritage ,archeology department http://www.ciram-
896 art.com/en/archaeology.html

897   ▪ Poznan Lab. Poznan Radiocarbon Laboratory, Poland, email: c.fourteen@radiocarbon.pl
898   http://radiocarbon.pl/index.php?lang=en.
899   ▪ Beta Analytic radiocarbon dating, Miami, Florida, USA http://www.radiocarbon.com/, e-mail:
900   lab@radiocarbon.com
901

902

903

904

905   Figure 1
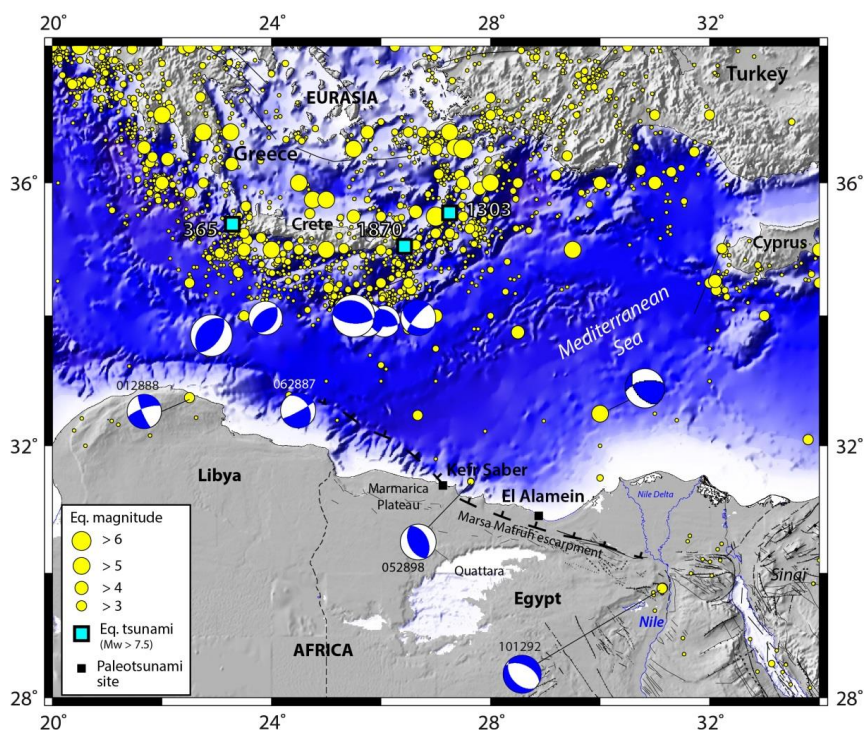
906

907

908

909

910   Figure 2

a   b

c
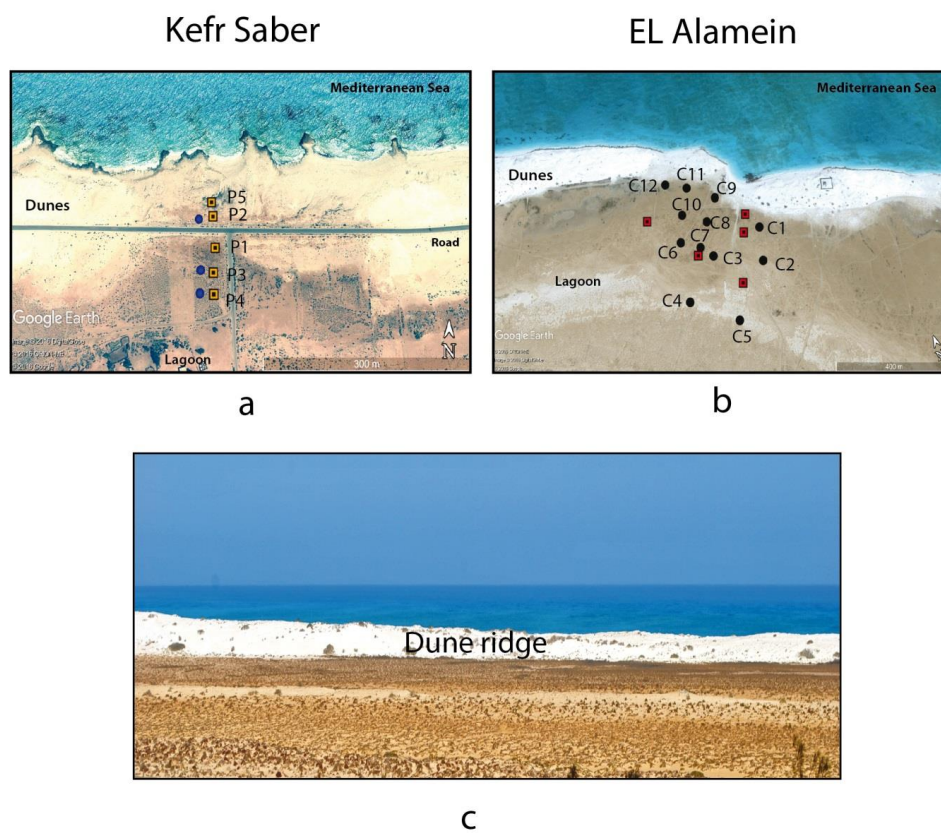
911

912

913

914   Figure 3
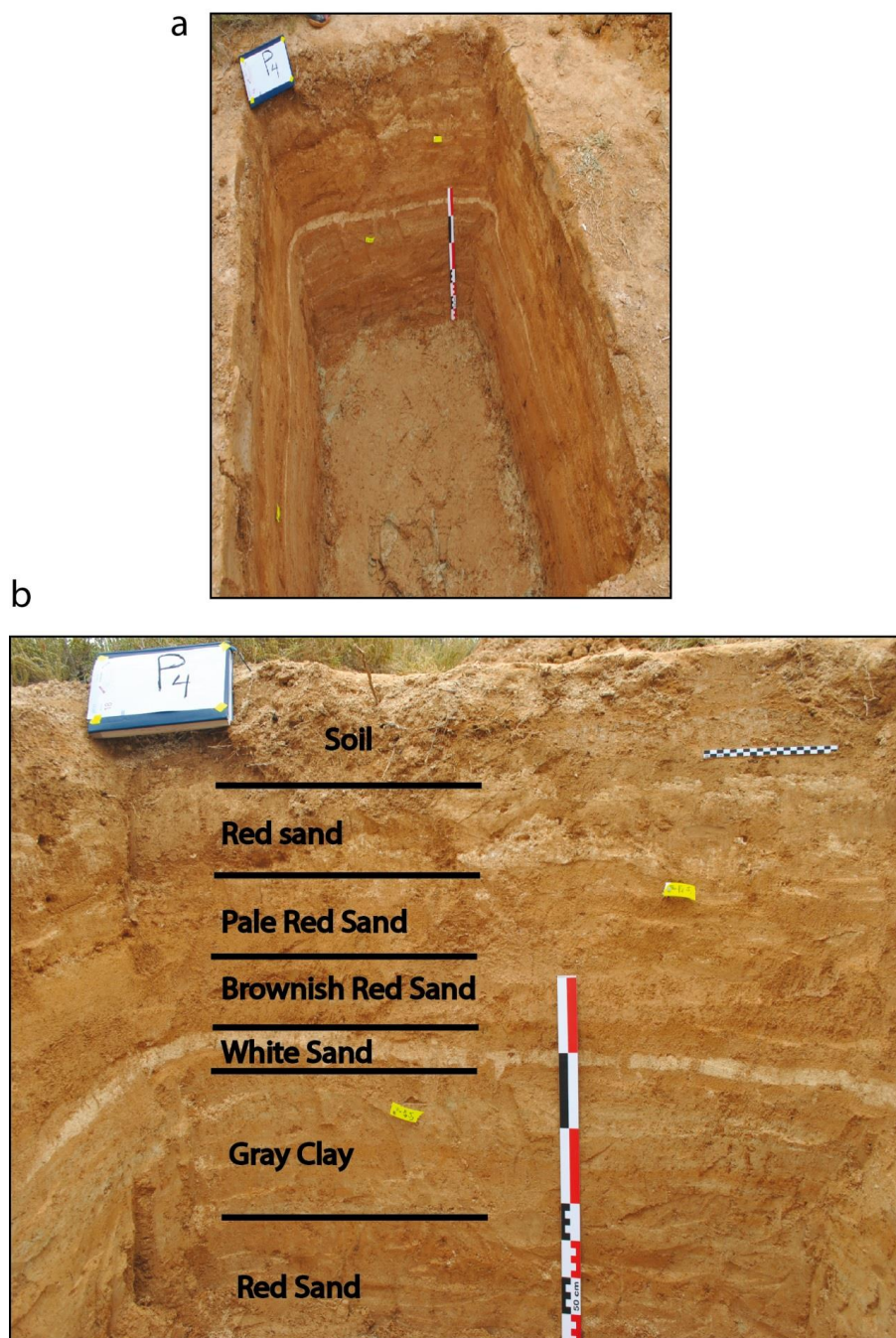
915

916

917

918   Figure 4

Kafr Saber

Radiocarbon dating of sedimentary units and tsunami deposit				Tsunami historical catalogue
Sample Name	Sample type	Cal.age (2σ)	Age Cal.	
TSU P3 S2	charcoal	820-1020 AD		
Simulated age of tsunami event X (137-422 AD)				Tsunami (21 July 365)
TSU P5S3	charcoal	30-180 AD		
TSU P3 S1	charcoal	49-59 AD		
TSU P5S4	charcoal	360-50 BC		
TSU P5S4	charcoal	1050-350 BC		
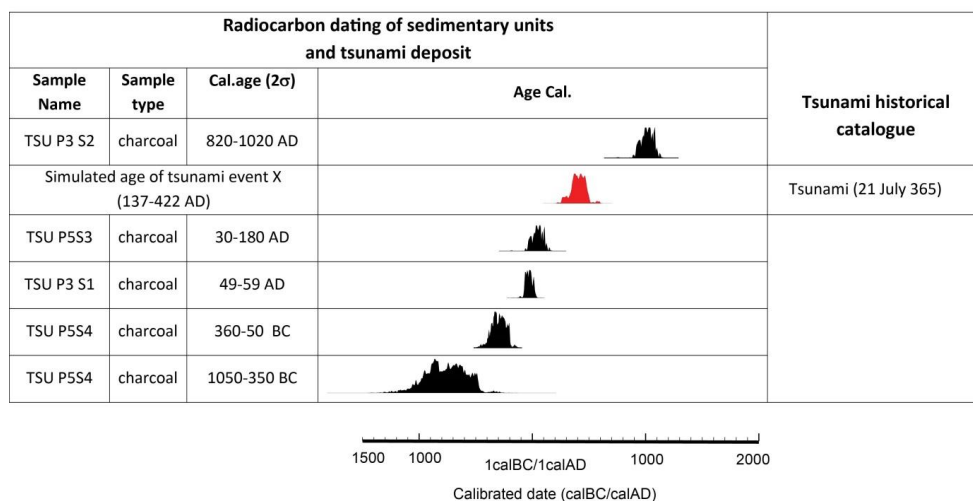
919

920

921

922   Figure 5 a
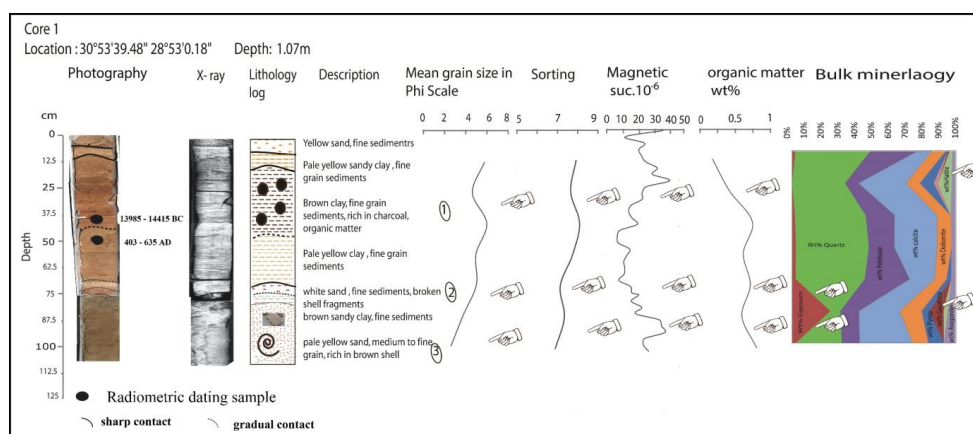
923

924

925

926

927   Figure 5 b
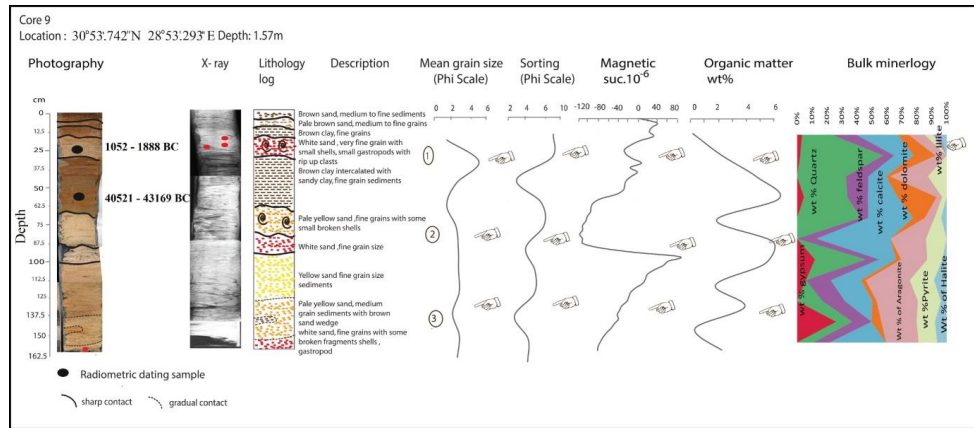
928

929

930   Figure 6
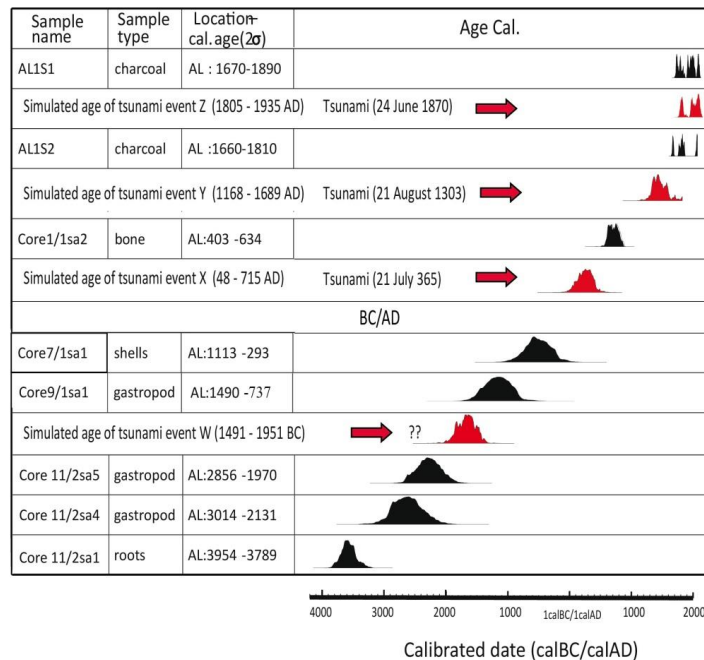
931

932

933   Figure 7

934

935

936

937